Appl Phys B (2011) 103: 137–144
DOI 10.1007/s00340-010-4175-7

Applied Physics B
Lasers and Optics

Broadening of upper polariton branch in GaAs, GaN, and ZnO semiconductor microcavities

S.-C. Lin · J.-R. Chen · T.-C. Lu

Received: 27 May 2010 / Published online: 24 August 2010

Abstract The well-distinguished lower polariton branches (LPBs) and upper polariton branches (UPBs) are characteristics of strong coupling in semiconductor microcavities (MCs). In practice, however, the UPBs are often broadening especially in wide-bandgap material MCs. We present in detail the possible physical mechanisms for the broadening of UPBs for different designs of MCs by numerical simulations based on GaAs, GaN and ZnO materials. The calculated results show that the UPBs of the GaN- and ZnO-based MCs will become indistinct when the thickness of optical cavity is larger than λ and 0.25λ, respectively, mainly attributed to the larger product of the absorption coefficient and the active layer thickness. In wide-bandgap materials, it would be relatively easier to observe the UPB in the case of negative exciton-cavity mode detuning due to the exciton-like UPB and lower absorption of scattering states. In addition, the inhomogeneous broadening would be an important factor causing the invisible UPB in wide-bandgap semiconductor MCs. We demonstrate that in multiple quantum well embedded ZnO-based MCs, the UPB could be well defined due to the large 2D exciton binding energy and the small product of absorption coefficient and active layer thickness. These results show that the UPBs can be properly defined in wide-bandgap semiconductor MCs by appropriate design of the MC structures.

S.-C. Lin · J.-R. Chen · T.-C. Lu (✉)
Department of Photonics & Institute of Electro-Optical Engineering, National Chiao Tung University, Hsinchuo, 300, Taiwan
e-mail: timtclu@mail.nctu.edu.tw
Fax: +886-3-5716631

1 Introduction

Since 1992, studies of strong light-matter interaction in semiconductor microcavities (MCs) have been started with the pioneering work of Weisbuch et al. [1]. By performing reflectivity measurements, the strong coupling between the exciton resonance and the confined photon cavity mode was discovered, which makes semiconductor MCs an interesting issue due to the enhanced control of light-matter interaction in solid-state systems. In the strong coupling regime, a new quasi-particle termed cavity–polariton will be created and characterized by bosonic properties, very small effective mass, as well as controllable dispersion curves. Through these unique properties of MC polaritons, the investigations on fundamental physical phenomena and advanced optoelectronic devices are reported in recent years, such as Bose-Einstein condensates [2, 3], parametric amplifications [4], solid-state cavity quantum electrodynamics [5], and polariton light-emitting diodes [6]. However, these literatures reported the prominent results in GaAs- and CdTe-based MCs obtained at cryogenic temperature. To achieve polariton devices operating at room temperature (RT), it is necessary to direct the interest toward wide-bandgap semiconductors as a result of their large exciton binding energy and large oscillator strength, such as the III-V compound GaN and II-VI compound ZnO [7].

The strong-coupling regime has been widely studied in the domain of atomic physics [8]. The physical mechanism of strong coupling for an atom in an optical cavity is relatively simpler than that for excitons in a semiconductor MC since it does not involve the strong relaxation phenomena observed in a solid-state system. Therefore, the two eigenstates of upper polariton and lower polariton are identical in amplitude and linewidth for the case of an atom in a high-finesse cavity. On the contrary, for exciton resonances

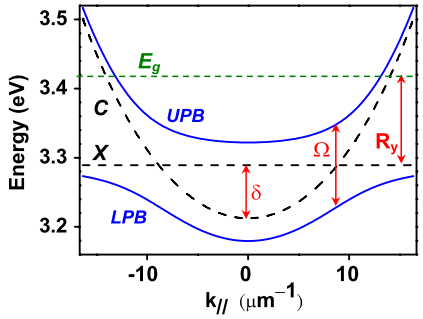

Fig. 1 Typical polariton dispersion inclusive of the upper polariton branch (UPB) and lower polariton branch (LPB), represented by *blue lines*. The pure cavity mode C, exciton mode X (*black dashed line*) and band edge E_g are shown (*green dashed line*). These symbols δ, Ω, and R_y represent exciton-cavity mode detuning, Rabi splitting, and Rydberg energy

in a semiconductor MC, there can be interactions between polaritons and excited states of excitons. Additionally, the exciton continuum states may have a large impact on the polariton eigenstates when the Rabi splitting is equal to or larger than the exaction binding energy in the strong-coupling regime [9]. Specifically, the absorption resulting from the continuum states causes broadening of the upper polariton state and leads to blurred polariton dispersion curves.

Figure 1 shows typical cavity-polariton dispersion curves in the case of negative detuning (i.e., the exciton energy is larger than cavity photon energy at zero in-plane wave vector). The cavity-polariton dispersion exhibits a lower polariton branch (LPB) and an upper polariton branch (UPB). When the energy of UPB is higher than the band edge of bulk active layer (the horizontal green dashed line) with increasing in-plane wave vector, the exciton continuum states would broaden the UPB in the energy range indicated by the blue dashed lines. There are three important parameters determining the relationship between UPB and exciton continuum states: the Rabi splitting (Ω), the effective Rydberg energy of excitons (R_y) or exciton binding energy, and the exciton-cavity mode detuning (δ). When the Rabi-splitting value is of the same order as or larger than the effective Rydberg energy, the UPB will be pushed up to the energies of the exciton scattering states, and then upper polaritons scatter with exciton scattering states, which leads to strong damping of the upper polaritons. Furthermore, it is relatively easy to cause the UPB to cross with the exciton continuum states in the condition of large positive exciton-cavity mode detuning. Therefore, these above-mentioned internal physical mechanisms will have different importance depending on the structure design and active layer materials.

To well define the existence of the strong-coupling regime in semiconductor MCs, the simultaneous appearance of LPB and UPB is strong evidence from the view point of experimental measurements. For this reason, the possible impacts on the visibility of UPB should be further discussed. In this study, we intend to compare the behaviors of UPB and the optical spectra for bulk GaAs-, GaN-, and ZnO-based MCs. We employ the approaches based on transfer matrix method and improved Lorentz oscillator model, including exciton continuum absorption and exciton inhomogeneous broadening, to analyze the specialties of reflectivity spectra for these three materials. The appropriate designs of the active layer thickness and the exciton-cavity mode detuning are investigated in order to suppress the absorption of exciton scattering states for UPB. In addition, we also point out that the exciton inhomogeneous broadening plays an important role for the visibility of UPB particularly in current wide-bandgap semiconductor MCs. In the last part of this paper, we investigate whether the coherence of UPB is still damped by exciton continuum states in multiple-quantum-well-based ZnO MCs. These calculation results shall be valuable for the comparison with experimental results in GaAs-, GaN-, and ZnO-based MCs.

2 Comparison of UPB broadening between microcavities based on different materials

For simplicity, the MC structures are composed of the same dielectric SiO_2/HfO_2 Bragg mirrors and the active layer is based on the bulk GaAs, GaN, or ZnO, respectively. In addition, it is noteworthy that there are two compensating layers symmetrically on the both sides of the active layer, as shown in Fig. 2(a). These two layers are added in the optical cavity to satisfy the cavity thickness of $m\lambda/2$, where m is the number of cavity mode. Based on this design structure, we can obtain the mapping of the reflectivity spectra of MCs with continuous variable active layer thicknesses. We have to emphasize that the two compensating layers are not taken into account in strong light-matter interaction. Figure 2(b) shows the refractive index profile and the optical-field intensity in the vertical direction. Moreover, the number of DBR layers is adjusted to keep the cavity quality factor the same for the pure cavity mode.

In the calculation, we only considered the excitonic transition from fundamental state ($1s$) based on the assumption of probing the polariton properties of wide-bandgap materials (GaN and ZnO) at RT. In addition, the oscillator strength of ns excited states is inversely proportional to n^3 [10], with n being the principle quantum number. Therefore, the excited states contribute only minor interaction with cavity photon modes. On the other hand, since excitons in GaAs are unstable and hardly exist at RT, we employed the relevant parameters obtained from the experimental measurements at cryogenic temperature for GaAs material [11]. The linewidths of exciton resonances are characterized by the same homogeneous broadening of 1 meV in the three materials in order to clear the specificities and differences. The

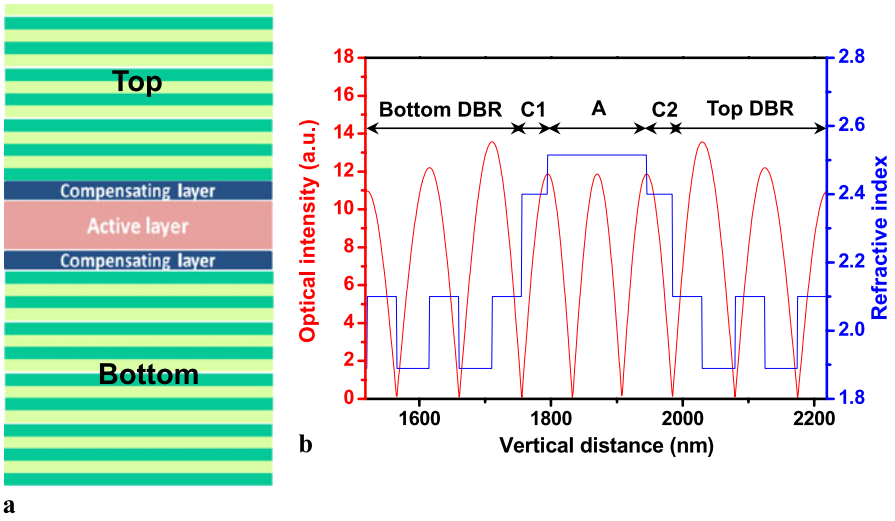

Fig. 2 (**a**) Schematic diagram of the bulk semiconductor microcavity. (**b**) Refractive index profile and the optical-field intensity in the vertical direction of the microcavity structure. A and C1 (C2) represent the active layer and compensating layer, respectively

Table 1 Relevant parameters of GaAs, GaN, and ZnO microcavities

	GaAs	GaN	ZnO
Refractive index	3.57	2.73	2.52
Exciton transition energy	1.515 eV	3.477 eV	3.286 eV
Rydberg	4.1 meV	26.6 meV	59 meV
$\alpha(E_g)$	1.0×10^4 cm^{-1}	1.1×10^5 cm^{-1}	2.0×10^5 cm^{-1}
Bohr radius	13 nm	3.1 nm	1.8 nm

similar results are obtained for larger homogeneous broadening (∼15 meV).

The reflectivity spectra of the MCs for three materials were calculated based on transfer matrix method [12] and the resonant exciton was modeled by a Lorentz oscillator dispersive dielectric function [13]. Besides, in order to take the exciton continuum states into account, the 3D exciton physical model is used in our calculation to involve the absorption of bound states and scattering states, which can be described as [14]

$$\alpha(\hbar\omega) = \frac{A_0}{2\pi^2 R_y a_0^3}\left[4\sum \frac{\gamma/n^3}{(\chi + 1/n^2)^2 + \gamma^2} + \int \frac{d\chi'}{\pi} \frac{\gamma S_{3D}(\chi')\sqrt{\chi'}}{(\chi - \chi')^2 + \gamma^2}\right], \quad (1)$$

where A_0 is proportional to the momentum matrix element of bulk semiconductors, R_y is the exciton Rydberg energy, a_0 is the exciton Bohr radius, γ is the half-linewidth normalized by Rydberg, χ is a normalized energy $(\hbar\omega - E_g)/R_y$, and S_{3D} is called the Sommerfeld enhancement factor and can be expressed as

$$S_{3D}(\chi) = \frac{2\pi/\sqrt{\chi}}{1 - e^{-2\pi/\sqrt{\chi}}}. \quad (2)$$

Table 2 Calculated Rabi-splitting values and corresponding active layer thickness in GaAs, GaN, and ZnO microcavities

	GaAs	GaN	ZnO
Active layer thickness (1λ)	230 nm	130 nm	150 nm
Rabi splitting (Ω)	4 meV	30 meV	70 meV

The corresponding parameters of the three materials were extracted from the literatures [15–20] and summarized in Table 1. By employing the 3D exciton model, we can define the scattering absorption including continuum states and excitonic absorption. The calculated results for the three materials are consistent with the absorption spectra reported by Refs. [16–18].

2.1 Influence of the active layer thickness

In bulk semiconductor MCs system, the Rabi splitting is strongly dependent on the thickness of cavity layer since the whole cavity can be referred to as the active material. Therefore, it is expected that the Rabi splitting will increase with the thickness of the cavity layer due to the increased overlap between matter and confined photons [15]. Generally, the Rabi splitting in a semiconductor MC can be described by [21]

$$\Omega = 2\sqrt{\omega_0 \omega_{LT}(d/L_{eff})}, \quad (3)$$

where ω_0 is the exciton resonance energy, ω_{LT} the effective longitudinal-transverse splitting, d the active layer thickness, and L_{eff} the effective cavity thickness involving the optical-field penetration in distributed Bragg reflectors (DBRs). An increase in Rabi splitting is obtained with increasing the active layer thickness of bulk cavity due to the larger ratio d/L_{eff} [11].

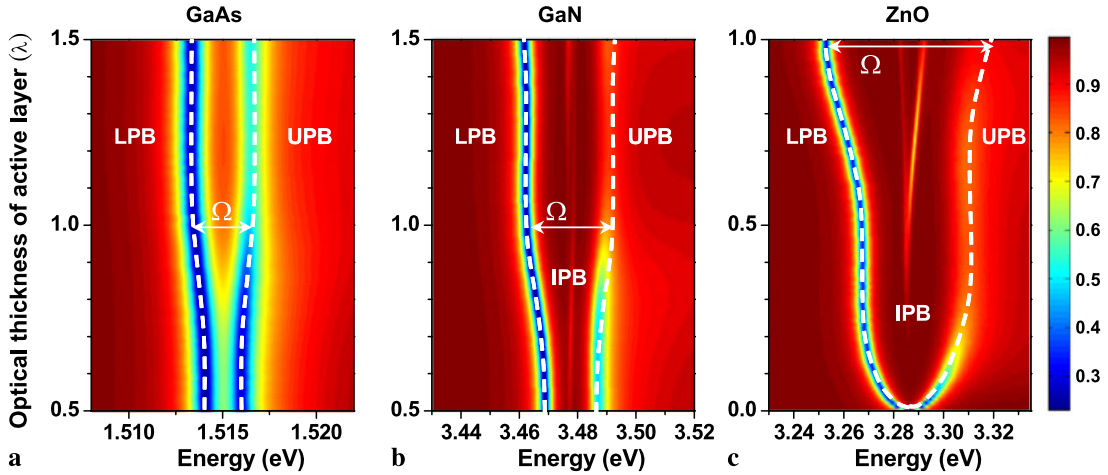

Fig. 3 Color maps of calculated reflectivity spectra as a function of active layer thickness for GaAs, GaN, and ZnO MCs at zero detuning and normal incidences. The *white dashed lines* show the UPB and LPB without considering exciton continuum absorption

Figure 3 presents the color maps of reflectivity spectra as a function of the active layer thickness for GaAs, GaN, and ZnO MCs, respectively. The reflectivity spectra were calculated in the condition of zero detuning and normal incidence ($k_{//} = 0$). The calculated Rabi-splitting values for the three MCs with optical thickness of 1λ are listed in Table 2. In Fig. 3, it is apparent that there are two main branches, the UPB and LPB, for these three MC structures and the Rabi splitting becomes larger with increasing active layer thickness. It is worthy to mention that the Rabi splitting near the 0.5-λ optical thickness of active layer shows approximately constant (i.e., the UPB and LPB are nearly parallel), which originates from the small increase in the exciton-photon interaction due to the node of the optical field in the MC structure. In the GaAs-based MCs, since the Rabi spitting is comparable to the effective Rydberg energy, as shown in Tables 1 and 2, the UPB is broader than the LPB with increasing Rabi splitting because of its crossing with the scattering states of excitons. Nevertheless, it is still distinguishable even that the optical thickness of the active layer is 1.5λ [11]. Furthermore, the UPBs of GaN and ZnO become broader with increasing thickness of active layer and subsequently fade as the optical thickness of about 1λ and 0.25λ for GaN and ZnO, respectively. These calculated results are in good agreement with the experimental measurements in recent literature [19, 22–25]. It is obvious that the maximum thickness of active layer for the visible UPB is different in the three materials. To clearly probe the UPB in ZnO MCs, the optical thickness of active layer should be kept thinner than 0.25λ to suppress the absorption of scattering states, which may mainly originate from the onset of continuum absorption and the exciton-phonon complexes, especially at RT [26]. Moreover, there are observable intermediate polariton branches (IPBs) in the map of the calculated reflectivity spectra nearby and above the exciton energy for GaN and ZnO MCs. This issue will be discussed further in Sect. 2.3.

In addition, the important factor resulting in the discrepancies between the three materials is the product of the absorption coefficient and the active layer thickness ($\alpha \cdot d$). The absorption coefficients near the band edge of GaN and ZnO are about one order of magnitude larger than that of GaAs, as shown in Table 1. Specifically, a bulk GaAs with an optical thickness of 1.5λ will absorb 49% of photons in a single pass when the photon energy is near the onset of the continuum states. As for a bulk ZnO with an optical thickness of 1λ, there is 95% of photons absorbed by the continuum states. To sum up the influence of the active thickness, when the thickness of bulk active layer increases, there are two mechanisms leading to the invisible UPBs for the wide-bandgap materials. One is the large Rabi splitting with increasing active layer thickness, which pushes the UPB into the absorption of scattering states. The other is the increased absorption induced by the increase in the thickness of bulk active layer.

2.2 Influence of exciton-cavity mode detuning

The effect of exciton-cavity mode detuning dominates the polariton dispersion curves and therefore influences the characteristics of UPB. It has been observed that the linewidth of the upper polariton increases with positive detuning due to the overlap between exciton scattering states and UPB in GaAs-based MCs [27, 28]. Furthermore, semi-classical approach of linear dispersion theory including the continuum absorption presents the similar trend about detuning-dependent UPB linewidths [29]. Therefore, to further investigate the effect of exciton-cavity mode detuning on the properties of UPB in these three materials, we fixed the optical thickness of active layer to be 0.5λ for

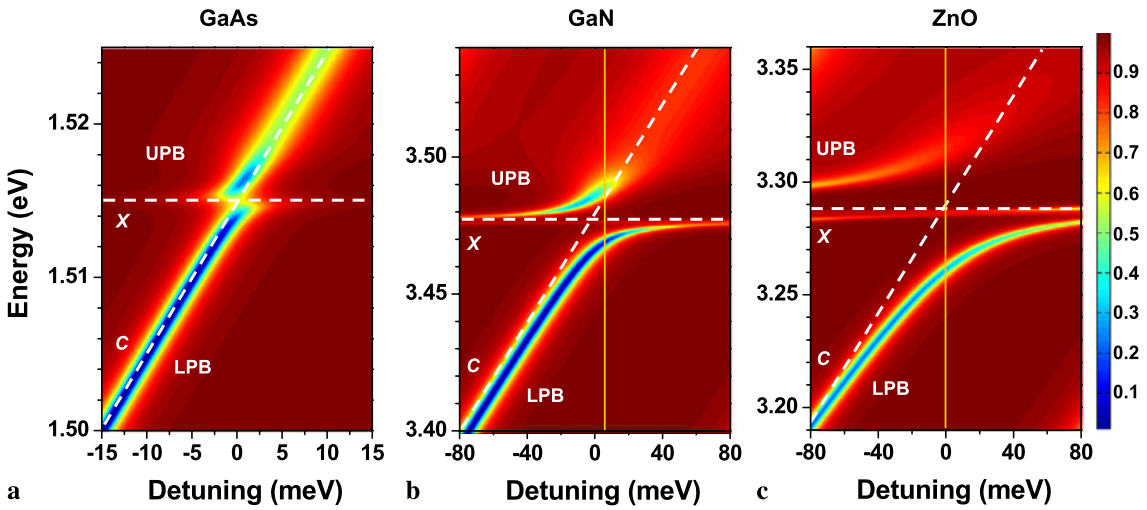

Fig. 4 Color maps of calculated reflectivity spectra as a function of exciton-cavity mode detuning for GaAs, GaN, and ZnO MCs with λ active layer thickness at normal incidence. The pure cavity mode *C* and uncoupled exciton mode *X* are shown (*white dashed line*). The vertical yellow line represents the critical value of detuning for invisible UPB

the three MCs and slightly changed the cavity thickness to increase or decrease the exciton-cavity mode detuning. Figure 4 shows the color maps of the calculated reflectivity spectra as a function of exciton-cavity mode detuning for the three materials. A clear anticrossing behavior is observed for GaAs- and GaN-based MCs, respectively. Nevertheless, when the exciton-cavity mode detuning deviates from the zero detuning, the signature of the exciton-like polariton branches disappears rapidly in the GaAs MC. On the contrary, in the cases of GaN and ZnO MCs, the exciton-like polariton branches are still visible for the large negative and positive detuning since their exciton oscillator strength values are one order larger than that of GaAs [13, 15, 30]. Furthermore, although anticrossing can be observed in the GaN MC, the signature of the UPB nearly disappears when the positive detuning is larger than about 10 meV. Similar situation also can be found in the ZnO MC when the detuning goes from negative to zero. For positive detuning, the upper polariton has high photon fractions, leading to the invisible UPB abruptly with increasing positive detuning due to the crossing with exciton scattering states. The UPB in GaAs MC is still distinct because the small term of $\alpha \cdot d$, as shown in Fig. 3(a). Therefore, in wide-bandgap materials it would be relatively easier to observe the UPB in the case of negative exciton-cavity mode detuning, besides the thinner active layer thickness as discussed in Sect. 2.1.

2.3 Influence of inhomogeneous broadening

Inhomogeneous broadening of excitons plays an important role in the investigation of strong exciton-photon coupling as well, especially for wide-bandgap materials due to the difficulty in growth of high reflectivity DBRs and high *Q* cavities. The effect of disorder on bulk polaritons results from the interaction between exciton states and imperfect bulk crystals. This mechanism breaks the conservation rule of in-plane wave vector in the exciton-photon interaction. As a result, the set of the disordered potential contributes to inhomogeneous broadening for the exciton-like polariton states in spectra. Currently, the epitaxial growth of wide-bandgap materials suffers from the severe strain accumulation in the DBRs, leading to crystal defects and potential fluctuations. Additionally, the small effective Bohr radius in wide-bandgap materials causes the polaritons more probably to be trapped by defects and perturbed by potential fluctuations, which results in the coherence length of polaritons to be significantly reduced.

As mentioned in the previous section, the calculated reflectivity spectra, as shown in Fig. 3, exhibit clear intermediate branches between the LPB and UPB. The IPBs are mainly resulted from the strong changes in the refractive index and the incoherent exciton absorption owing to the outcome of large exciton oscillator strength. However, these IPBs have never been observed experimentally in GaN- or ZnO-based MCs [23, 25]. Furthermore, although the results shown in Fig. 4 present visible UPBs with sharp linewidth in the range of negative detuning for the three materials, the most experimental results in reflectivity and photoluminescence spectra exhibit the broad linewidth of UPB [23, 25]. These differences are mainly attributed to the lack of inhomogeneous broadening in the calculation model. Therefore, in order to take the effect of inhomogeneous broadening into account, the simulation models are reconstructed from a convolution of a Lorentzian lineshape and a Gaussian lineshape, which is more appropriate in the case of inhomogeneous broadening. The exciton Gaussian lineshape is

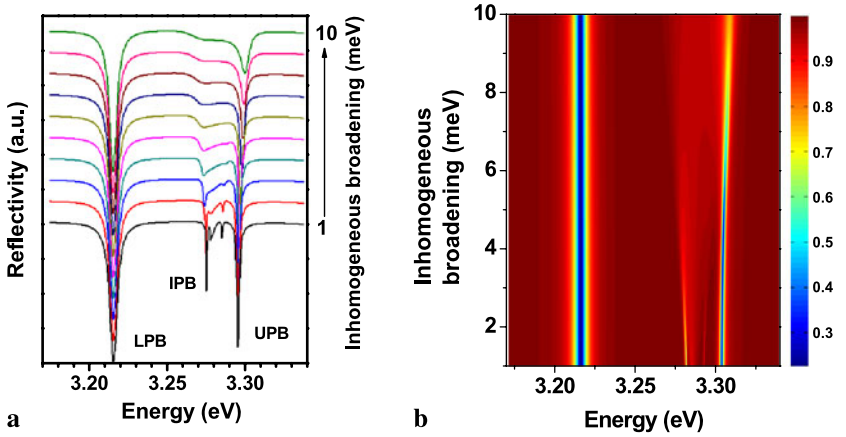

Fig. 5 (**a**) Calculated reflectivity spectra for the λ ZnO cavity at zero detuning and zero in-plane wave vector as varying the inhomogeneous broadening ranging from 1 to 10 meV. (**b**) Color map of the reflectivity spectra as a function of inhomogeneous broadening

symmetrically distributed in our work to avoid the breaking of translational symmetry and to modify the polariton eigenstates [31].

The calculated results shown in Fig. 4 indicate that the UPBs in the range of positive detuning are significantly broadened by the absorption of exciton scattering states. As for the UPBs in the range of negative detuning, the inhomogeneous broadening will be the dominant mechanism leading to the invisible UPBs due to the exciton-like polaritons. Figure 5(a) shows the calculated reflectivity spectra for the λ ZnO cavity in the condition of negative detuning of 50 meV and zero in-plane wave vector as varying the inhomogeneous broadening ranging from 1 to 10 meV. Figure 5(b) presents the color map of the reflectivity spectra as a function of inhomogeneous broadening. The LPB is clearly distinguishable even if the inhomogeneous broadening increases to be 10 meV. However, the intermediate dips (i.e., IPBs) resulting from the incoherent excitons rapidly vanish with increasing inhomogeneous broadening, and finally the UPB becomes blurred and fades as the inhomogeneous broadening approaches 10 meV. The disappearance of UPB with increasing inhomogeneous broadening is mainly induced by the intrinsic exciton-like properties for the condition of negative detuning. On the contrary, the LPB is photon-like and therefore robust in spite of the increase of inhomogeneous broadening. Consequently, the inhomogeneous broadening induced by crystal imperfection would also be an important factor causing the invisible UPB in wide-bandgap semiconductor MCs.

3 Comparison between QWs-embedded and bulk ZnO-based MCs

The above-discussed studies of strongly exciton-photon coupling are mainly based on bulk MCs because of the simpler geometry and the easier fabrication in practice, especially for wide-bandgap materials. However, with the target of realizing an electrically pumped polariton laser, a more realistic structure would employ QWs to achieve lower threshold due to improved carrier confinement and large oscillator strength. Recently, the strong coupling based on a GaN/AlGaN multiple-quantum-well (MQW) MC structure has been experimentally demonstrated [32]. Nevertheless, the ZnO-based MQW MCs, such as ZnO/ZnMgO, have not been reported. Therefore, we will now focus on the comparison of polariton dispersion curves in bulk ZnO and ZnO/ZnMgO MQW MCs.

The MC structures for the bulk ZnO and ZnO/ZnMgO MQW are identical except for the design of cavities. The cavity thickness of these two structures is 0.5λ and the MQW structure consists of three 3-nm ZnO QWs and 5-nm $Zn_{0.73}Mg_{0.27}O$ barriers, which are symmetrically distributed around the anti-node of the optical field. In addition, the variations of exciton transition and binding energies in a $ZnO/Zn_{0.73}Mg_{0.27}O$ QW as a function of well width have been investigated in the work by Coli and Bajaj [33]. The measured transition energy in a QW structure consisting of a 3-nm-thick ZnO well and $Zn_{0.73}Mg_{0.27}O$ barriers is about 3.39 eV [33, 34].

Figure 6 shows the comparison of the angle-resolved reflectivity spectra ranging from −35° to 35° between MQW and bulk ZnO-based MCs. In Fig. 6(a), it is obvious that the MQW ZnO-based MC presents an evident UPB. Therefore, it is easy to estimate the value of Rabi splitting. On the contrary, in the bulk ZnO MC the upper polariton is blurred and completely fades as a result of the intense damping by scattering states. The main factors resulting in the difference between MQW MC and bulk MC are essentially attributed to two reasons. One is the product of the absorption coefficient and the cavity thickness ($\alpha \cdot d$). In the QWs-embedded MCs this value is effectively reduced because of the thinner active layer thickness. To be more specific, the product ($\alpha \cdot d$) in a single pass is about 0.36 in the case of QWs-embedded MCs, which is about ten times less than that in bulk ZnO MCs (~ 3.0). The other is the difference in exciton binding energies. The QW structure is supposed to

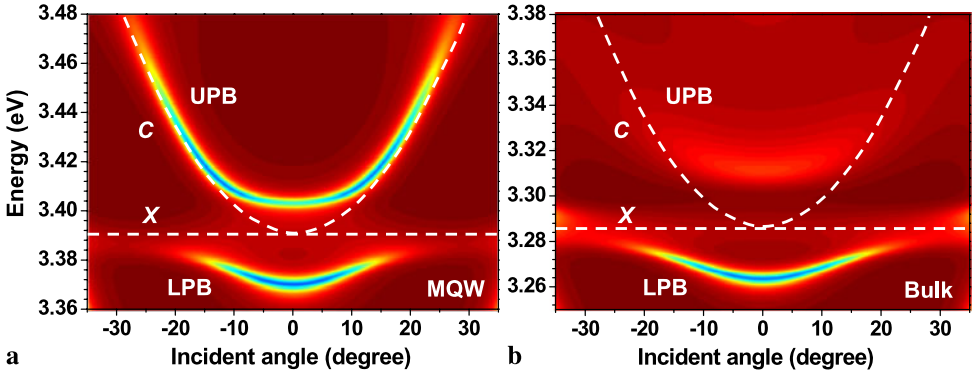

Fig. 6 Color maps of the calculated angle-resolved reflectivity spectra of 0.5-λ (**a**) MQW ZnO-based MC, (**b**) bulk ZnO-based MC

have larger exciton binding energy than bulk active layer. For ideal 2D QW structure, the exciton binding energy is expected to be 4 times larger than that in bulk active layer [14]. However, the practical QW is a quasi-2D structure since the wave functions of electron and hole are confined in the direction normal to the wafer surface in a finite well width, which implies that the exciton binding energy in a quasi-2D QW is smaller than that in an ideal 2D QW. Additionally, the quantum confined Stark effects in c-axis ZnO QWs can shift the absorption peak and reduce exciton binding energies. Consequently, we assume the exciton binding energy of the ZnO/ZnMgO QW to be 99 meV in our calculation [35]. Under this condition, the exciton continuum states will be much far from the UPB, which is another benefit for the MQW ZnO-based MC in order to probe the visible UPB.

4 Conclusion

In conclusion, we have presented the numerical simulation about the investigation of different physical mechanisms inducing the broadening of UPB in semiconductor MCs based on three different materials. According to the simulation results, the UPBs of the GaN- and ZnO-based MCs will become indistinct when the thickness of optical cavity is larger than λ and 0.25λ, respectively. The invisible UPBs are mainly dominated by the product of the absorption coefficient and the active layer thickness. Furthermore, it is preferred to probe a visible UPB in the case of negative exciton-cavity mode detuning since the UPB in positive detuning is photon-like and induces decoherence by exciton scattering states, especially for wide-bandgap MCs. There is still a clear UPB in GaAs-based MC with thick bulk active layer due to the smaller absorption coefficient than that in wide-bandgap materials. In addition to the active layer thickness and exciton-cavity mode detuning impact on the broadening of UPBs, the inhomogeneous broadening induced by crystal imperfection would also be an important factor causing the invisible UPB in wide-bandgap semiconductor MCs. Finally, we demonstrated the potential for MQW ZnO-based MCs to improve the visibility of UPB due to the large 2D exciton binding energy and the small product of absorption coefficient and active layer thickness. Therefore, the employment of MQW ZnO-based MCs and the improvement of wide-bandgap material quality will be necessary to observe the well-defined strong-coupling regime and even to achieve low-threshold polariton devices.

Acknowledgements This work was supported in part by the MOE ATU program and in part by the National Science Council of the Republic of China under Contracts NSC 96-2221-E009-092-MY3, NSC 96-2221-E009-093-MY3, and NSC 96-2221-E009-094-MY3.

References

1. C. Weisbuch, M. Nishioka, A. Ishikawa, Y. Arakawa, Phys. Rev. Lett. **69**, 3314 (1992)
2. J. Kasprzak, M. Richard, S. Kundermann, A. Baas, P. Jeambrun, J.M.J. Keeling, F.M. Marchetti, M.H. Szymañska, R. André, J.L. Staehli, V. Savona, P.B. Littlewood, B. Deveaud, L.S. Dang, Nature **443**, 409 (2006)
3. R. Balili, V. Hartwell, D. Snoke, L. Pfeiffer, K. West, Science **316**, 1007 (2007)
4. M. Saba, C. Ciuti, J. Bloch, V. Thierry-Mieg, R. André, L.S. Dang, S. Kundermann, A. Mura, G. Bongiovanni, J.L. Staehli, B. Deveaud, Nature **414**, 731 (2001)
5. K.J. Vahala, Nature (Lond.) **424**, 839 (2003)
6. S.I. Tsintzos, N.T. Pelekanos, G. Konstantinidis, Z. Hatzopoulos, P.G. Savvidis, Nature **453**, 372 (2008)
7. M. Zamfirescu, A. Kavokin, B. Gil, G. Malpuech, Phys. Status Solidi (a) **195**, 563 (2003)
8. R.J. Thompson, G. Rempe, H.J. Kimble, Phys. Rev. Lett. **68**, 1132 (1992)
9. S. Faure, T. Guillet, P. Lefebvre, T. Bretagnon, B. Gil, Phys. Rev. B **78**, 235323 (2008)
10. R.J. Elliott, Phys. Rev. **108**, 1384 (1957)
11. A. Tredicucci, Y. Chen, V. Pellegrini, M. Böger, L. Sorba, F. Beltram, Phys. Rev. Lett. **75**, 3906 (1995)
12. R.M.A. Azzam, N.M. Bashara, *Ellipsometry and Polarized Light* (North-Holland, Amsterdam, 1977)
13. N. Ollier, F. Natali, D. Byrne, P. Disseix, M. Mihailovic, A. Vasson, J. Leymarie, F. Semond, J. Massies, Jpn. J. Appl. Phys. **44**, 4902 (2005)
14. S.L. Chuang, *Physics of Photonic Devices*, 2nd edn. (Wiley, New Jersey, 2009), pp. 679–680
15. Y. Chen, A. Tredicucci, Phys. Rev. B **52**, 1800 (1995)

16. M.D. Sturge, Phys. Rev. **127**, 768 (1962)
17. J.F. Muth, J.H. Lee, I.K. Shmagin, R.M. Kolbas, H.C. Casey, B.P. Keller, U.K. Mishra, S.P. DenBaars, Appl. Phys. Lett. **71**, 2572 (1997)
18. G.E. Jellison, L.A. Boatner, Phys. Rev. B **58**, 3586 (1998)
19. J.-R. Chen, T.-C. Lu, Y.-C. Wu, S.-C. Lin, W.-R. Liu, W.-F. Hsieh, C.-C. Kuo, C.-C. Lee, Appl. Phys. Lett. **94**, 061103 (2009)
20. R. Johne, D.D. Solnyshkov, G. Malpuech, Appl. Phys. Lett. **93**, 211105 (2008)
21. V. Savona, L.C. Andreani, P. Schewndimann, A. Quattropani, Solid State Commun. **93**, 733 (1995)
22. F. Réveret, F. Médard, P. Disseix, J. Leymarie, M. Mihailovic, A. Vasson, I.R. Sellers, F. Semond, M. Leroux, J. Massies, Opt. Mater. **31**, 505 (2009)
23. R. Butté, G. Christmann, E. Feltin, J.-F. Carlin, M. Mosca, M. Ilegems, N. Grandjean, Phys. Rev. B **73**, 033315 (2006)
24. F. Médard, J. Zuniga-Perez, P. Disseix, M. Mihailovic, J. Leymarie, A. Vasson, F. Semond, E. Frayssinet, J.C. Moreno, M. Leroux, S. Faure, T. Guillet, Phys. Rev. B **79**, 125302 (2009)
25. R. Shimada, J. Xie, V. Avrutin, Ü. Özgür, H. Morkoč, Appl. Phys. Lett. **92**, 011127 (2008)
26. W.Y. Liang, A.D. Yoffe, Phys. Rev. Lett. **20**, 59 (1968)
27. R. Rapaport, A. Qarry, Solid State Commun. **120**, 387 (2001)
28. J.R. Jensen, P. Borri, W. Langbein, J.M. Hvam, Appl. Phys. Lett. **76**, 3262 (2000)
29. M. Maghrebi Mellitia, R. Chtouroua, J. Blockb, V. Thierry-Miegb, Physica E **30**, 17 (2005)
30. F. Médard, J. Zúñiga-Perez, E. Frayssinet, J.C. Moreno, F. Semond, S. Faure, P. Disseix, J. Leymarie, M. Mihailovic, A. Vasson, T. Guillet, M. Leroux, Photon. Nanostruct. Fundam. Appl. **7**, 26 (2009)
31. V. Savona, C. Piermarocchi, Phys. Status Solidi (a) **164**, 45 (1997)
32. G. Christmann, R. Butté, E. Feltin, J.-F. Carlin, N. Grandjean, Appl. Phys. Lett. **93**, 051102 (2008)
33. G. Coli, K.K. Bajaj, Appl. Phys. Lett. **78**, 2861 (2001)
34. K. Koike, G.-Y. Takada, K. Fujimoto, S. Sasa, M. Inoue, M. Yano, Physica E **32**, 191 (2006)
35. R.T. Senger, K.K. Bajaj, Phys. Rev. B **68**, 205314 (2003)